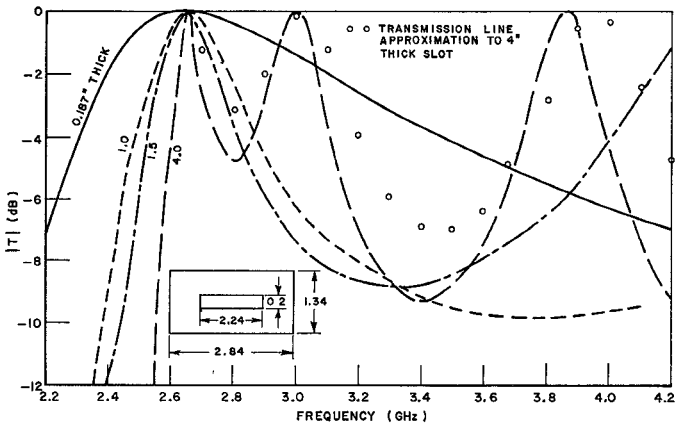

Fig. 8. Calculated values of the transmission coefficient versus frequency for 0.2-in-wide rectangular slots of various thicknesses in a waveguide.

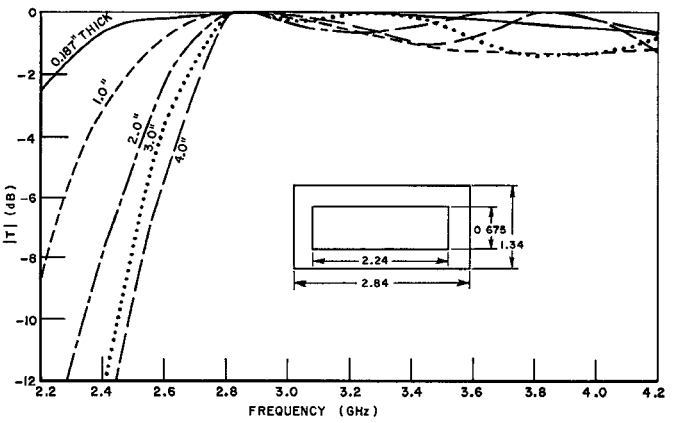

Fig. 9. Calculated values of the transmission coefficient versus frequency of 0.675-in-wide rectangular slots of various thicknesses in a waveguide.

in Fig. 8. For thick slots ($l > \lambda$), simple transmission line calculations can yield reasonably accurate results. The transmission line calculations shown in Fig. 8 were made by using the TE_{10} mode characteristic impedances [6] and neglecting the higher order modes at junctions 1 and 2.

It is evident that the slot shown in Fig. 9, if filled with dielectric to lower its cutoff frequency, would have the expected transmission characteristics of a waveguide pressure window.

Conclusions

The modal analysis method of Wexler can be used to calculate the reflection and transmission properties of thick rectangular waveguide windows. However, for thick, finitely conducting waveguide windows, the method loses accuracy because of mode coupling due to surface resistance. By modifying the modal propagation constants so as to include these effects, significant improvement in accuracy is obtained. This same technique can no doubt be used to more accurately treat other finitely conducting waveguide obstacles.

Acknowledgment

The authors wish to thank Prof. L. Peters, Jr., for the many helpful suggestions that he made concerning this work.

References

[1] L. Lewin, *Advanced Theory of Waveguides*. New York: Iliffe, 1951, pp. 21, 88–97.
[2] N. Marcuvitz, *Waveguide Handbook*. New York: McGraw-Hill, 1951, pp. 248–257, 404–408.
[3] A. Wexler, "Solution of waveguide discontinuities by modal analysis," *IEEE Trans. Microwave Theory Tech.*, vol. MTT-15, pp. 508–517, Sept. 1967.
[4] R. E. Collin, *Field Theory of Guided Waves*. New York: McGraw-Hill, 1960, pp. 193, 230.
[5] R. F. Harrington, *Time-Harmonic Electromagnetic Fields*. New York: McGraw-Hill., 1961, p. 73.
[6] E. C. Jordan and K. G. Balmain, *Electromagnetic Waves and Radiating Systems*. Englewood Cliffs, N. J.: Prentice-Hall, 1968, p. 264.

Negative TEO–Diode Conductance by Transient Measurement and Computer Simulation

HANS L. HARTNAGEL AND MITSUO KAWASHIMA

***Abstract*—A new method based on slow microwave transients due to steep bias-voltage steps gives a detailed negative-device-conductance function versus microwave-voltage amplitude v_{ac} for Gunn diodes. Measurements of GaAs and InP devices made by different fabrication processes as used by a variety of manufacturers show that basic differences in behavior exist. Some of these are representative of high switching speeds and others of good steady-state efficiencies. Computer simulation of Gunn devices with a range of mobility and ionized-donor density profiles oscillating in a suitable resonant structure leads to similar differences in negative-conductance functions. A first correlation between experimental and theoretical behavior is attempted, and it is possible to estimate the mobility and carrier-density profiles which could most likely be responsible for a certain device behavior.**

It is shown that an external locking signal affects the device's negative conductance only for small values of v_{ac}, and experimental results confirm that this, in accordance with theoretical expectation, increases the switching speed only of certain types of diodes.

Manuscript received November 16, 1973; revised January 21, 1973. This work was supported by the Science Research Council.

The authors are with the Department of Electrical and Electronic Engineering, University of Newcastle upon Tyne, Newcastle upon Tyne, England.

I. Introduction

FOR SEVERAL years now, transferred-electron oscillators (TEO's) have been available. They are in widespread use for numerous applications. Unfortunately, it is difficult to establish the actual semiconductor space-charge mode for a particular device producing microwave oscillations, especially as a whole range of space-charge modes is possible with nl around 10^{12} cm^{-2}, where n is the ionized-donor density and l is the length of the active layer. Each mode can cause a different type of behavior, which has to be selected in accordance with the requirements of any application. Whereas some space-charge modes, such as the LSA mode, are possible only with certain RF circuits, the normally found TEO modes are only determined by such parameters as the conductivity profile, and therefore the fabrication processes employed which should be correctly chosen for the application envisaged. Thus a method of systematically characterizing transferred-electron devices of different fabrication processes is of value, particularly if information can be derived concerning the space-charge mode present.

Many details of behavior are expressed by the device's negative conductance g_d as a function of microwave voltage v_{ac} across the device terminals. One can derive such details as the output power for a given load conductance, the efficiency, the switch-on transients, and the output-amplitude stability for load or bias supply fluctuations. Hitherto, this device conductance has been obtained by measuring the microwave impedance loading the device under steady-state operation [1] or by quenching oscillations by suitable loading and determining the device impedance by reflection techniques. The latter technique, however, does not necessarily result in the same results, as the severe loading required for stabilization can strongly affect the space-charge mode of the semiconductor. Additionally, the large negative conductance over a wide frequency range exhibited by a good Gunn diode has made it difficult to employ this technique. The first technique, on the other hand, can only give results for a decreasing $|-g_d|$ versus v_{ac} range, where stable operation is possible.

A more suitable technique has recently been proposed by the authors [2]. This relies on the measurement of the transient wave for a very sharp bias-voltage step applied. The function $|-g_d|$ versus v_{ac} can be obtained from the output-voltage transient function $v_o(t)$, where t is the time, after the relevant quality factors of the resonant circuit and the transformer ratio of $v_o/v_{ac}=n$ have been determined by independent measurements. This method requires that the transient wave take a long time with respect to a period of the microwave so that each amplitude value of the transient can be approximated as a steady-state case. Several further conditions have to be satisfied by the circuitry, such as single and constant frequency operation during transient, a minimum of harmonic content, and no change in the microwave-cavity mode (whereas space-charge wave mode changes can and do occasionally occur during one transient). Additionally, the bias pulse transient must be much shorter than the microwave transient so that the bias-voltage step can be approximated to be instantaneous.

This technique has now been employed systematically for a variety of transferred-electron devices from different manufacturers. Additionally, a computer program solving the continuity and Poisson equations for a range of doping and mobility profiles of Gunn diodes in suitable resonant circuits was used to calculate theoretical transients. The program was also employed to determine from the steady-state condition the corresponding $g_d(v_{ac})$ function by applying several load values. The possibility of allocating to an experimental $g_d(v_{ac})$ its corresponding theoretical function should then produce a means of determining the type of space-charge mode occurring in a particular diode. A first approach to this task is described in this paper. As the $g_d(v_{ac})$ behavior strongly depends on doping and mobility profiles which are determined by the fabrication processes, it should be possible to establish the optimum fabrication process for a certain device application

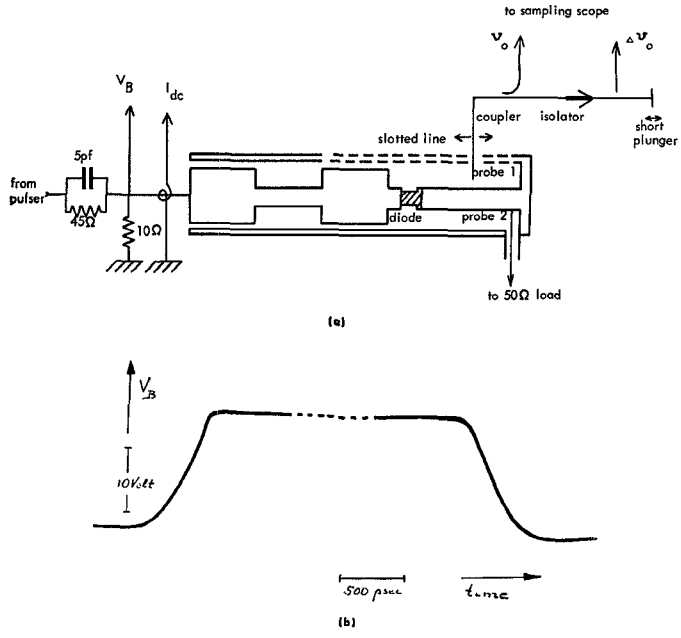

Fig. 1. Experimental system. (a) Resonator with Gunn-effect diode, together with pulse-steepening RC network, 10-Ω resistive impedance transformer, bias-current and voltage probes, low-pass filter, and two microwave probes. The weakly coupled movable probe 1 is connected to the sampling oscilloscopes and to a correlation system for the frequency measurement during transient. Probe 2 is fixed and strongly coupled. (b) Bias pulse experienced by the diode. This pulse is measured by probe 1 touching the filter section near the diode.

II. The Oscillator Model and its Equation

A coaxial cavity is employed, as shown in Fig. 1(a). Probe 1 is movable and is very lightly coupled; it monitors the microwave-field mode of the cavity. Probe 2 is tightly coupled and represents the load. The bias-voltage pulse experienced by the diode is given by Fig. 1(b). The cavity with the diode in its housing and with the load of probe 2 can be represented by an equivalent circuit as shown in Fig. 2. The energy-conservation equation leads then to the equation of an oscillator in terms of various quality factors and the output voltage v_o across the load, namely

$$\frac{d\ln v_o}{dt} = -\frac{\omega_0}{2}\left(\frac{1}{Q_d}+\frac{1}{Q_o}+\frac{1}{Q_{ex}}\right) \tag{1}$$

$$= -\frac{\omega_0}{2}\frac{1}{Q_t}. \tag{2}$$

Here, ω_0 is the angular frequency of oscillation, Q_d is the quality factor expressing the coupling of the negative-conductance device with the cavity, Q_o is the unloaded quality factor of the cavity, and Q_{ex} is the external Q giving the

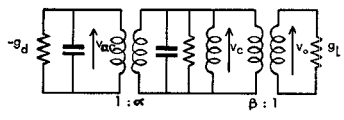

Fig. 2. Equivalent circuit of resonator with Gunn diode.

coupling of the load with the cavity. Q_l is the total Q of the system. For growing oscillations, Q_l must be negative, while it is positive for decaying output. With v_c, the RF voltage of the cavity, one finds two coupling coefficients α and β as defined by Fig. 2:

$$v_c = \alpha v_{ac} \tag{3}$$

$$v_c = \beta v_o. \tag{4}$$

This enables one to give the definitions of the quality factors in terms of the components of the equivalent circuit of Fig. 2, namely

$$\frac{1}{Q_d} = \frac{g_d}{C\omega_0\alpha^2} \tag{5}$$

$$\frac{1}{Q_{ex}} = \frac{g_l}{C\omega_0\beta^2}. \tag{6}$$

Here, C is the equivalent capacitance of the total microwave circuit, which includes the device's capacitance transformed to the cavity. As the device's capacitance depends on the voltage v_{ac}, a change in frequency during the transient time can be expected. Both computer studies and experimental investigations (see the Appendix), have shown that this frequency variation is negligible because the device's capacitance is very small in comparison with the equivalent cavity capacitance. It is, however, necessary to establish that the frequency variation during transients for each of the diodes characterized is below an acceptable limit. A convenient method for this purpose is described in the Appendix.

Equations (1), (2), and (5) also give a condition for oscillations to be able to start after the bias voltage V_B has been increased above threshold. This condition means that for small $v_{ac}(=(\beta/\alpha)v_o)$, Q_l must be negative. This means, $|-g_d|$ in (5) must be sufficiently large for the values of Q_o and Q_{ex}. For heavy loading (large g_l or small β), oscillations can be inhibited. Often, $|-g_d|$ has a maximum value for a finite v_{ac}, where Q_l can be negative while it is positive for very small v_{ac}. Then oscillations can only be initiated by applying some external microwave signal, which has to be maintained until the transient wave has reached a value where Q_l becomes negative.

Inserting (3)–(6) into (1) gives a relation suitable for the derivation of g_d from the transient function v_o (time), i.e.

$$\frac{1}{v_o}\frac{dv_o}{dt} = -\frac{\omega_0}{2}\left(\frac{1}{n^2 Q_{ex}}\frac{g_d}{g_l} + \frac{1}{Q_l}\right) \tag{7}$$

where $n=\alpha/\beta$ and $1/Q_l = 1/Q_o + 1/Q_{ex}$.

III. Experimental Procedure

The $\lambda/2$ resonant cavity employed is made of a 50-Ω coaxial line with the device a distance $\lambda/8$ away from the two-stage filter blocking the microwaves, but permitting the passage of very steep bias pulses with a minimum of distortion (in Fig. 1, λ is the wavelength of the microwave along the coaxial line). The bias-pulse slopes are steepened by an RC network before being applied to the filter. At the entrance to the filter, a disk resistor of a few ohms acts like an impedance transformer and ensures that the diode is biased by a supply source with small internal resistance. The bias-voltage pulses are generated by an Hg-wetted-relay pulser involving a 50-Ω cable. The bias voltage and current are monitored at the entrance to the filter. The loosely coupled sliding probe is positioned in a slot, which is filled in by two sliding metal bars on either side of the probe so that only a minimum of mode distortion is ensured.

The rise and decay times of oscillations are measured directly on a sampling oscilloscope (HP 141 A). In order to establish the frequency responses of it above 10 GHz, this was measured carefully by comparison with a power meter The oscilloscope is triggerable up to 18 GHz, but around 15 GHz several resonances occur where the reflection coefficient at the input is rather high. However, there were a few short ranges of frequency where matching was observed to the 50-Ω line. A mismatch can distort the measured waveshape due to multiple reflections. This can be partly overcome by high-quality attenuators. However, it was decided to use only those frequency ranges where matched conditions existed. The width of such a frequency range had to be larger than the inverse of the transient time of the microwaves.

In order to reduce the harmonic content of the output, the diode was positioned in the cavity in such a manner that the first harmonic coupling coefficient between the diode and cavity was small, i.e., the first and other uneven harmonic frequencies could no longer experience any useful negative conductance. This is possible by placing the diode along the coaxial line such that the diode impedance can be matched to the transmission-line impedance at the fundamental, but not at the first and other odd harmonic frequencies. Ideally, by placing the diode $3/8\lambda_1$, where λ_1 is the wavelength of the fundamental frequency, away from the shortened end of the $\lambda_1/2$ cavity, the diode experiences a reasonable circuit impedance at the fundamental frequency, whereas at the first harmonic it sees an impedance of infinite value. Some experimental observations made by varying the position of the diode tend to confirm this consideration.

Strong coupling is arranged between the load and cavity so that Q_l is small for the fundamental frequency and the transient times are long. This can, unfortunately, aid the harmonic-frequency buildup, and some compromise has to be made.

For the evaluation of the transient function v_o by (7), the parameters n, Q_{ex}, and Q_l have to be determined; g_l is known, as it is the 50-Ω characteristic impedance of the matched transmission line connected to probe 2. Q_l is obtained by measuring the transmission characteristics of the cavity across the two probes when the diode is replaced by a corresponding piece of metal. This technique assumes that probe 1 is very loosely coupled so that only probe 2 affects the frequency response of the transmission characteristic. From the half-power width of the frequency characteristic of the transmission, Q_l can be derived. Q_{ex} is found by measuring the locking range of the oscillator to an external signal; n is found as follows: g_d is measured for steady-state conditions, when the left-hand side of (7) is zero. Equation (7) can then be employed to find n. The steady-state determination of g_d cannot be carried out by careful recording of the shape of the standing-wave pattern near the diode in the $\lambda/2$ cavity and subsequent derivation of the device's impedance, as the "near field" of the active device distorts the standing-wave pattern.

Instead, the following method is used: the real part R_L of the impedance of the loading probe to the cavity was expressed in terms of Q_l and the characteristic impedance of the coaxial line of the cavity by assuming that the cavity losses are included in the load R_L and that the standing-wave pattern of $\lambda/2$ is approximately of the same length as the cavity. The position of the maximum of the standing-wave pattern in the cavity is then measured very carefully. The distance from the short-circuited end of the cavity (opposite the filter termination) to this maximum gives the imaginary part of the loading impedance [caused by probe 2; see Fig. 1(a)] by using a Smith chart for the 50-Ω characteristic impedances of the resonator line. The distance from this end of the cavity to the position of the diode can then be employed to transform this load impedance to the reference plane of the diode, again using a Smith chart. The encapsulated-diode impedance then has the negative value of the transformed impedance. This method avoids the difficulty with the near field, as no measurements have to be made where the near field exists. Rather, the impedance is determined by a measurement of Q_l and of the position of the field maximum where the near field is small. The active-device conductance is finally derived by taking the equivalent circuit of the S4 package into account [3]. An estimate of the accuracy of this steady-state g_d measurement gives about ± 20 percent. It is pointed out here, however, that the basic details of the shape of the $g_d(v_{ac})$ characteristics are not influenced by any error of the steady-state g_d value which affects only the level of the conductance function.

Another method of finding $1/n^2Q_{ex}$ with (7) is based on the use of the decay of v_o for the bias-voltage termination. Then g_d is the low-field microwave conductance of the diode (which can be approximated by the low-field dc resistance R_0). It is essential here to use the trail of the decay transient in order to avoid any large-signal effects of the zero-biased diode. The results thus obtained agree to within about ± 20 percent with those of the above methods of determining n and Q_{ex} separately.

The output amplitude v_o is recorded by the sampling oscilloscope connected to a good X–Y plotter. Using (7) and the measured value of n, $g_d(v_{ac})$ is found. Extreme care is required in order to avoid any distortion of v_o, as this would falsify the results. In particular, the following precautions are therefore taken.

The applied bias pulse is made to be as smooth as possible while maintaining short rise times. In order to match the diode to the bias supply, an impedance-transforming disk resistor of 10 Ω at the entrance to the filter [see Fig. 1(a)] is given approximately the same value as the diode low-field resistance. Similarly, any mismatch between the output probe [either probe 1 or 2 of Fig. 1(a)] and the input to the sampler distorts v_o due to multiple reflections. Omni-spectra miniature (OSM) attenuators have not been found entirely satisfactory here and HP APC7 fixed attenuators with a rated bandwidth up to 18 GHz are used. All connectors and adaptors used are checked by using time-domain reflectometry. The accuracy for small v_{ac} values is poorer, as the derivation of $(1/v_o)(dv_o/dt)$ amplifies, than any error that might be present.

IV. Experimental Results

Numerous diodes of different manufacturers were investigated. A selection of typical results is shown in Figs. 3–6. All diodes have an active-layer length $l \cong 10$ μm, $n \cong 10^{15}$ cm^{-3}, and a flat conductivity profile.

Fig. 3 shows that $|-g_d|$ is roughly inversely proportional

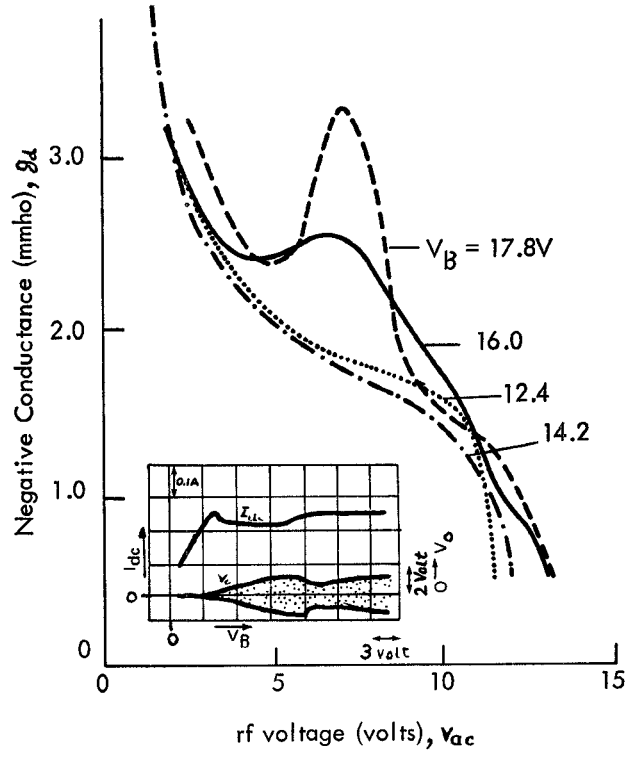

Fig. 3. $g_d(v_{ac})$ for a GaAs Gunn diode with metal alloyed cathode (low-field resistance of diode $R_0 = 9.2$ Ω, operating frequency $f_0 = 10.5$ GHz, device capacitance at $V_B = 14$ V—0.35 pF). The insert shows the dc current I_{dc} (upper trace) and the RF voltage v_o as a function of bias voltage V_B.

to v_{ac}. This diode has a large $|-g_d|$ at small v_{ac} and exhibits correspondingly a fast switch-on time. It would be suitable for applications where fast switching is essential. The efficiency and steady-state v_{ac} are not very high as $|-g_d|$ falls off rapidly with v_{ac}; $|-g_d|$ does not increase appreciably with bias voltage V_B, except where a second peak occurs above $V_B = 12$ V for $v_{ac} = 7$ V. This peak is representative of a different space-charge mode occurring in the diode, as also shown by the fact that the dc current drop for transferred-electron oscillations is decreased (see the upper trace of the insert in Fig. 3 for $V_B > 12$ V) and the RF output amplitude v_o is affected (see the lower trace of the insert in Fig. 3). If a load conductance is sufficiently high, two stable operating points can then be obtained, where the operation at the higher v_{ac} values is only possible by applying for a short period an external signal which brings v_{ac} above 8 V.

Fig. 4 shows, on the contrary, an almost constant $|-g_d(v_{ac})|$ relation. As the $|-g_d|$ values are small for small v_{ac} values, slow switch-on processes are found. This can be shortened considerably, effectively increasing the negative conductance, by injecting an external signal as shown in Section V. The dc current drop for this particular space-charge mode is small, as shown by the upper trace of the insert in Fig. 4. An increase in the bias voltage can result in a large increase in v_o. Both the efficiency and output power are high.

Fig. 5 shows an intermediate case. Here, a metal cathode produces results similar to those of the n^+ cathode of Fig. 4. Fig. 3 and 5 demonstrate that metal cathodes can either result in fast or slow switch-on speeds. From this point of view, metal cathodes can be equivalent to n^+ cathodes. There are, of course, other aspects of device behavior, such as noise and lifetime, when n^+ cathodes might be superior.

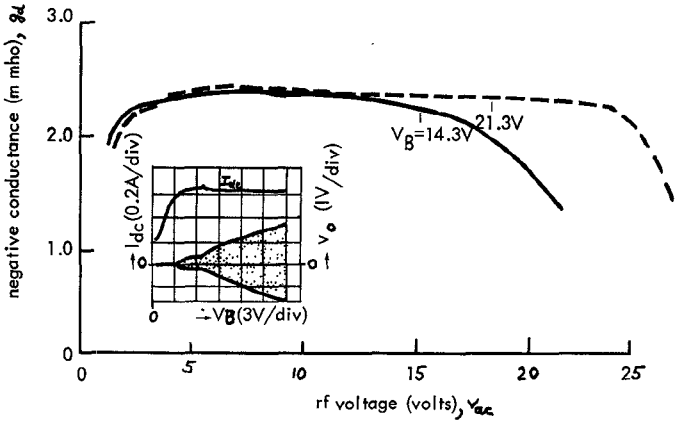

Fig. 4. $g_d(v_{ac})$ for a GaAs diode with n^+ cathode ($R_0=5.5\ \Omega$, $f_0=9.7$ GHz, device capacitance at $V_B=14$ V-1.06 pF). The insert shows I_{dc} and v_o as a function of V_B.

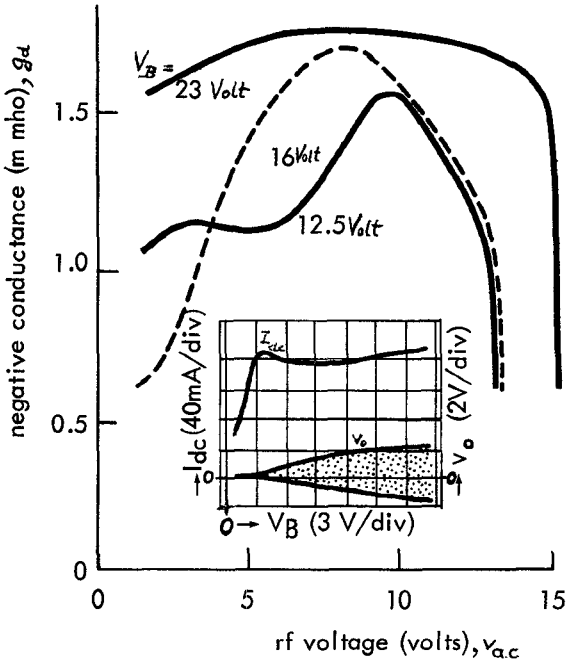

Fig. 5. $g_d(v_{ac})$ for a GaAs diode with metal alloyed cathode ($R_0=12.7\ \Omega$, $f_0=10.45$ GHz, device capacitance at $V_B=14$ V—0.30 pF). The insert shows I_{dc} and v_o versus V_B.

Regarding the InP diodes investigated, only metal cathodes are available. The two types of cathodes available basically exhibit a similar behavior as found with GaAs–metal cathodes, namely, either fast or slow switch-on speeds. The slow case is given with evaporated AgSn electrodes. These devices generally operate at J band. There is no sharp drop in bias–current–voltage characteristics. Two different space-charge modes are observed by altering the bias voltage. The two modes show different delay characteristics.

On the other hand, Sn dot cathodes on InP show a very fast rise time in both the X and J band and a clear current drop. The rise times of these diodes were so short that special precautions had to be taken, such as severe loading, in order to justify the assumptions involved with (7). Fig. 6 shows the corresponding negative conductance versus v_{ac}. It is seen that the values of $|-g_d|$ for small v_{ac} are extremely large. The

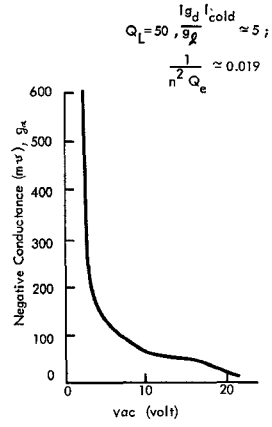

Fig. 6. $g_d(v_{ac})$ for InP diode with Sn dot cathode ($R_0=10\ \Omega$, threshold voltage—20 V, operating voltage—30 V, efficiency—2 percent, $f_0=15.82$ GHz).

frequency change of this particular diode for the bias-voltage range of 20–35 V is only about 150 MHz, and is indeed small for the frequency of oscillation.

V. Effective Increase in Negative Conductance by Injection Locking

It is known that an external signal applied to the diode during switch-on shortens the switching time. When this phenomenon is considered in terms of the effect on the $g_d(v_{ac})$ function, the experimental details of locking for individual diodes can be easily understood.

The circuit equation for a parallel resonant oscillator can be expressed as follows (also see [4]):

$$C\frac{dv_{ac}}{dt}+(g_l-g_d)v_{ac}+\frac{1}{L}\int v_{ac}\,dt=i(t) \qquad (8)$$

where $i(t)$ is the injection signal; C and L are the effective oscillator capacitance and inductance, respectively; and v_{ac} is the RF voltage. In the transient case and with $i(t)\neq 0$, the amplitude and phase of $v_{ac}(t)$ are time dependent. By assuming that the resonator Q is large, $v_{ac}(t)$ is nearly sinusoidal with slowly varying amplitude and phase. Expressing $v_{ac}(t)$ by a Taylor-series expansion and neglecting higher order terms, we can integrate (8) over the fundamental period. This leads to two equations: one for the amplitude $v_1(t)$ of the fundamental of v_{ac} and the other for the phase $\phi(t)$ of v_1. Assuming that the injected signal has the same frequency as the resonance of the circuit, one finds from the equation for $v_1(t)$ the relation

$$-\frac{1}{v_1}\frac{dv_1}{dt}=\frac{1}{2C}(g_l^*-g_d-g_i\cos\gamma) \qquad (9)$$

where g_l^* is the load conductance applied to the device, C is the resonator capacitance, g_i is the effective conductance of the injected signal, g_d is the negative conductance of the device, and γ is the phase difference between the injected signal and the oscillation voltage; g_i is given by the amplitude ratio of the injection current to the oscillation voltage: $g_i=i_0/v_1$. Equation (9) shows, therefore, that the injection signal has the effect of increasing the negative conductance of the device, thus decreasing the switch-on time. This would, however,

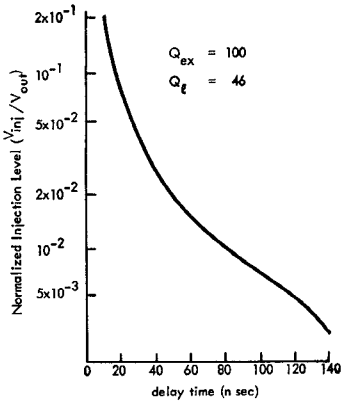

Fig. 7. Injection level versus resulting switch-on delay time of a GaAs diode for an external signal applied at the same frequency as the circuit resonance (V_{inj} is the injection-voltage amplitude across the 50-Ω line leading to probe 2 of Fig. 1; V_{out} is the steady-state output voltage from probe 2).

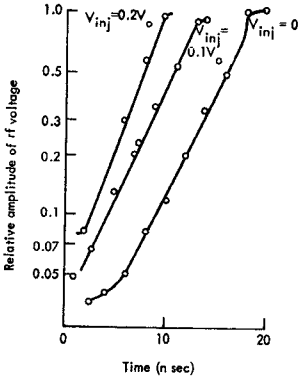

Fig. 8. Switch-on transient for different injection voltages V_{inj} for a GaAs diode

only have a strong effect for those ranges where g_a is smaller or of the same order of magnitude as $g_i \cos \gamma$.

Fig. 7 shows the experimental results for a diode with a large delay time (i.e., characteristics similar to that of Fig. 5) which is shortened considerably by an injection signal. A diode with a characteristic of Fig. 3 could, on the other hand, hardly show any increase in switching speed. Fig. 8 shows the transient functions for three different injection levels when using the same diode as for Fig. 7. One can see that the delay time is reduced by the injected signal, but that the growth rate is practically unchanged This shows that the effect of the injection signal is most pronounced for small v_{ac} ranges if diodes are employed which have a bell-shaped $g_d(v_{ac})$ function with small values near the origin.

VI. Computer Simulation and Evaluation of Results

By computing $g_d(v_{ac})$ for diodes with various doping and mobility profiles, it is hoped that a correlation between experimental and theoretical results will be found. This could then be used, first, to establish the profiles (and thus the fabrication processes) required for a given device application, and, second, to lead to a method of estimating the actual profiles of given diodes.

Two types of circuits are used, namely, a lumped and a distributed circuit (see Fig. 9). The latter one includes additional reactances in order to simulate the device's "cold"

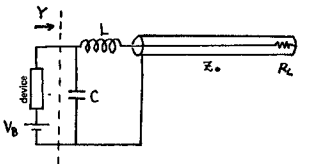

Fig. 9. Distributed circuit used for computation. L and C represent the reactances of the package and the unbiased device.

capacitance and package. The bias-voltage step is given by a cosine function, where the step time t_r has a realistic value of typically 200 ps The details of the circuits are chosen so that the harmonic frequencies of the bias-voltage step do not find any undesirable circuit resonance.

The diode is computed by solving the continuity equation and Poisson's equation, using a finite-difference method, with suitable initial and boundary conditions. The terminal voltages and currents of the device are determined by solving the circuit equations. For the distributed circuit, the voltages and currents of the forward- and backward-traveling waves are found for a TEM wave reflected with a reflection coefficient

$$\rho = \frac{-Z_0 + R_L}{Z_0 + R_L}$$

at the end of the coaxial line, where Z_0 is the characteristic impedance of the coaxial line and R_L is the load resistance as given by probe 2 of Fig. 1 and the losses of the cavity. The program takes into account the convergence requirements which are determined by the diffusion coefficient and the time and space increments Δt and Δx, respectively. The latter ones were chosen to be $\Delta x = 0.1$ μm and $\Delta t = 0.1$ ps.

The doping density is 10^{16} cm^{-3} in the anode and cathode electrodes and reduces over a distance of 1 μm to 10^{15} cm^{-3}, which is the doping level of an active distance of 10 μm. The low-field mobility in the contact areas is sometimes less than 4000 cm^2/V·s (indicated with results), from where it linearly increases over a distance varying from 1 to 4 μm to 8000 cm^2/V·s, which is the mobility of the active layer. The change over for the mobility and the doping density is not necessarily of the same length or at exactly the same position. The computation is one dimensional, but for the determination of the terminal currents a cross-sectional surface of 10^{-8} m^2 is taken. A doping notch of 0.8-μm length is sometimes incorporated in front of the cathode. This is indicated with the results. An instantaneous velocity versus field relation is employed, where the threshold field and the constant high-field saturation velocity of 10^5 m/s is assumed to be independent of low-field mobility. The diffusion constant is kept constant with $D = 0.02$ m^2/s, except where otherwise stated.

The program yields the device's voltage and current, as well as the electric field distribution in the active layer, i.e., the space-charge mode. The device's current and voltage are then Fourier analyzed up to the third harmonic, and the equivalent conductance and susceptance are obtained for each frequency as a function of v_{ac}.

The function $g_d(v_{ac})$ derived for diodes with a doping notch and with low-field mobilities of 8000 cm^2/V·s across both electrodes and the active layer is shown in Fig. 10 for three bias voltages. The negative conductance is very large for small v_{ac} and resembles the experimental results of Sn-dot InP diodes (Fig. 6). v_{ac} increases to a value which covers al-

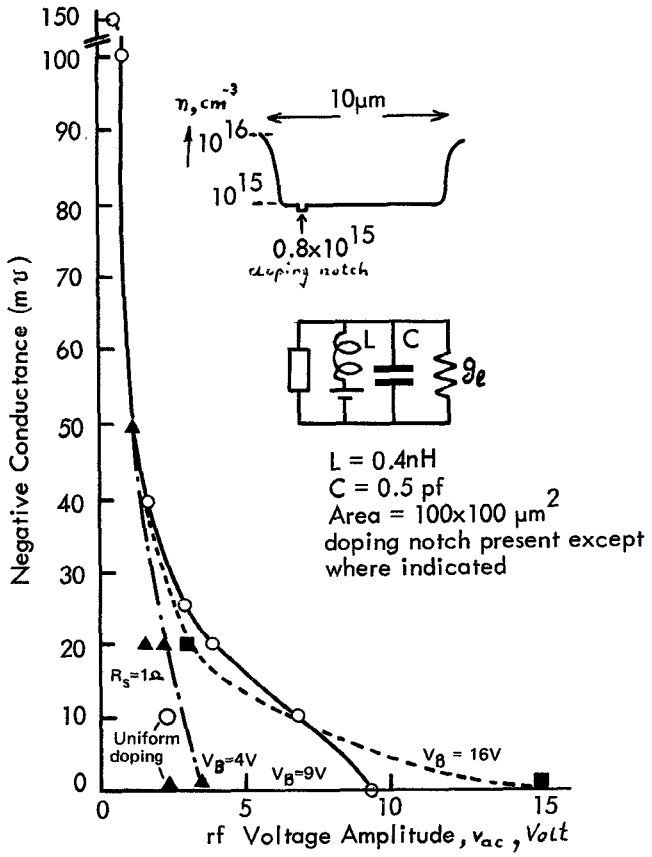

Fig. 10. Computed $g_d(v_{ac})$ for the doping profile, as shown by the top insert, and for the resonator representation, as shown by the lower insert. (○ and ○ ○ ○ are for $V_B=9$ V, ▲ and ▲—▲—▲ are for $V_B=4$ V, and ■ and ■—■—■ are for $V_B=16$ V. g_l is the load conductance of Fig. 2, transformed into the cavity with $\beta=1$.)

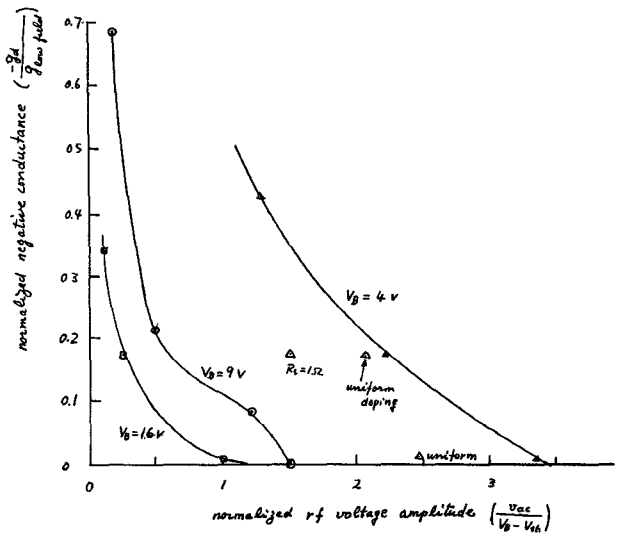

Fig. 11. Information of Fig. 10 in normalized form to demonstrate the large values of v_{ac} with respect to V_B. A delayed dipole mode is shown for $v_{ac}/(V_B-V_{th})<1$ and quenched dipole mode for $v_{ac}/(V_B-V_{th})>1$.

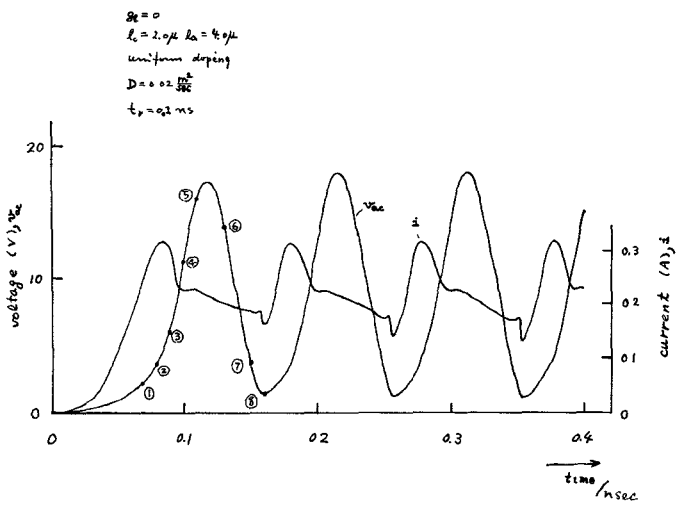

Fig. 12. Current and voltage transients for the linear low-field mobility decrease from 8000 to 4000 cm^2/V·s taking place over a distance l_c in front of the cathode and over a distance l_a in front of the anode (numbers refer to curves of Fig. 13; t_r is the transient time of V_B).

most the entire bias-voltage range. Fig. 10 also includes two points for a diode without a doping notch. These show that $|-g_d|$ at $v_{ac}=2$ V has decreased for $V_B=9$ V from 40 to 10 mΩ^{-1} and for $V_B=4$ V from 20 to 2 mΩ^{-1}. Additionally, there is one point for a series resistance $R_S=1\,\Omega$ to the device, which causes $|-g_d|$ to drop at $v_{ac}=2$ V from 50 to 20 mΩ^{-1}. The results of Fig. 10 with a doping notch are for an operation resembling the delayed-dipole domain mode.

For uniformly doped samples and constant mobilities, the initial mode of the switch-on transient is a traveling accumulation mode, operating over a few cycles. Subsequently, an additional stationary accumulation layer establishes itself near the anode. This reduces the traveling accumulation layer in amplitude. The traveling accumulation layer is able to produce a fast growth rate if the bias-voltage step is comparable or shorter than $t_r=100$ ps. Unfortunately, this condition is difficult to achieve experimentally. A computation for the circuit of Fig. 1(a) shows that the shortest bias-voltage step experienced by the diode with the filter and resonator used is only slightly less than $t_r=500$ ps [also see the experimental results of Fig. 1(b)]. Therefore, in reality the growth rates will normally be rather too slow for this switch-on mode to occur.

In order to demonstrate better the size of the voltage swing v_{ac} with respect to the bias voltage for the space-charge mode present in the diode, Fig. 10 is redrawn in normalized form (see Fig. 11). Note that for a small v_{ac} ($v_{ac}\leq V_B-V_{th}$, with V_{th} the threshold voltage for the TEO effect), a delayed dipole-domain mode is possible and shows a very large negative conductance. This may cause some difficulty in stabilizing such a diode for the operation as an amplifier.

Computations with a profile of reduced low-field mobilities inside the contacts and with the absence of a doping notch produce the following results. If a reduced mobility creates a low-field increase in front of the cathode, dipole domains are nucleated. Widening the reduced-mobility region near the anode and shortening it near the cathode causes a stationary high-field region to be established near the anode. This absorbs most of the traveling domain, which is partly dipole and partly accumulation layer. Fig. 12 shows the corresponding current and voltage function across the diode, whereas Fig. 13 shows the field profile along the diode for eight representative points of the switch-on transient. First, the formation of a stationary accumulation layer occurs as shown by curves ①–③ of Fig. 13. This is not associated with a noticeable reduction of microwave current for increasing voltage (see cor-

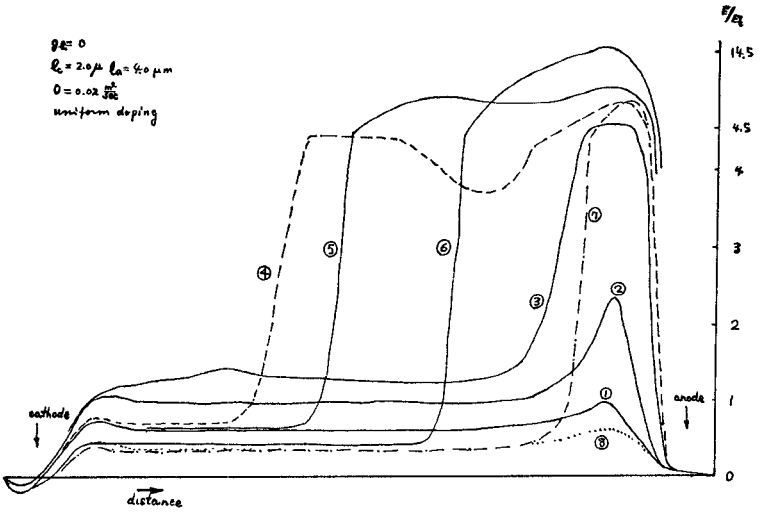

Fig. 13. Field profile along the diode of Fig. 12 with a mobility profile for eight points in time as defined by Fig. 12 (E—field, E_t—threshold field for the TE effect).

responding points ①–③ on Fig. 12). It illustrates that the stationary accumulation layer does not contribute very much to the device's negative conductance. The subsequently formed traveling accumulation domain (curves ④–⑦ in Figure 13), causes a large drop in current (see points ④–⑦ on Fig. 12), which primarily forms the negative conductance. The reduction in I_{dc} for this example above threshold is small, and is therefore analogous to the experimental results of Fig. 4.

In order to establish the amplitude of v_{ac} for a stationary domain only, i.e., its contribution to the negative conductance, the diode of Fig. 12 was given a length l_c of linear mobility decrease near the cathode of only 1 μm. The device's terminal current then had only an amplitude of 1.5 percent of the dc current, which is very small indeed. If the diode of Fig. 12 is additionally equipped with a doping notch near the cathode, a strong dipole domain is formed which dominates and prevents the stationary domain reaching any appreciable size (see Fig. 14). The current–voltage amplitude is then larger (see Fig. 15), except for the first cycle, where V_B had not yet reached its full value.

If the diffusion coefficient D is increased from 0.02 to 0.04 m²/s in the sample of Fig. 12, the nucleation of a dipole domain is entirely suppressed, and only a stationary accumulation layer exists near the anode. The resulting negative conductance is then very small. During the transient time, a temporary occurrence of a large-signal switching mode is sometimes found, which is followed by the low-conductance mode.

These computational results can be summarized as follows. A reduced-mobility region near the anode or an increased diffusion constant decreases $|-g_d|$, whereas a reduced mobility region near the cathode or a doping notch increases $|-g_d|$.

Finally, it should be mentioned briefly that with our computations, an improvement in switching speed is found to be possible by carefully selecting suitable harmonic resonances of the circuit.

VII. Conclusions

Measurements of the negative conductance versus microwave voltage across Gunn devices by slow transients in a specially designed circuit yield experimental details which cannot be obtained satisfactorily by any other method. In particular, the positive slopes of the $|g_d(v_{ac})|$ function can be determined, which are essential for a treatment of transient phenomena with the active device represented by an equivalent circuit of lumped elements.

A systematic experimental investigation of Gunn diodes of numerous manufacturers, both with GaAs and InP, have exhibited fundamental differences in g_d behavior. One type of result shows large $|g_d|$ for small v_{ac} with a rapid decrease of $|g_d|$ for increasing v_{ac}. These devices are suitable for fast switching operation. Computer simulation has shown that they can be associated with dipole domains due to the existence of a low-field mobility decrease or a doping notch near the cathode. Another type of $g_d(v_{ac})$ function shows a small $|g_d|$ for small v_{ac}. This increases to quite high values for increased v_{ac} before it finally decreases. One has devices suitable for high efficiencies and large output powers, but slow transients.

Computationally, the effects of doping and mobility profiles and of the diffusion constant on the $g_d(v_{ac})$ function are studied, and a correlation between experimental and theoretical data is attempted. This method can be employed by comparing experimental and computational behavior to establish the space-charge mode operating in a device. This then results in a selection of the fabrication process giving the doping and mobility profile required for optimum operation of a particular application.

It is shown how injection of an external signal increases the overall effective negative conductance for small v_{ac} ranges only, as the contribution to the negative conductance made by the injection signal is inversely proportional to v_{ac}. The switching behavior of diodes with different types of g_d characteristics under the influence of a locking signal is studied experimentally and can be explained in terms of the resulting effective conductance.

Appendix

Assessment of Frequency Change During Transient

An important assumption of the experimental method described here is that the frequency remains approximately constant during the transient times [see (1), for example]. However, the device's RF capacitance can be expected to be

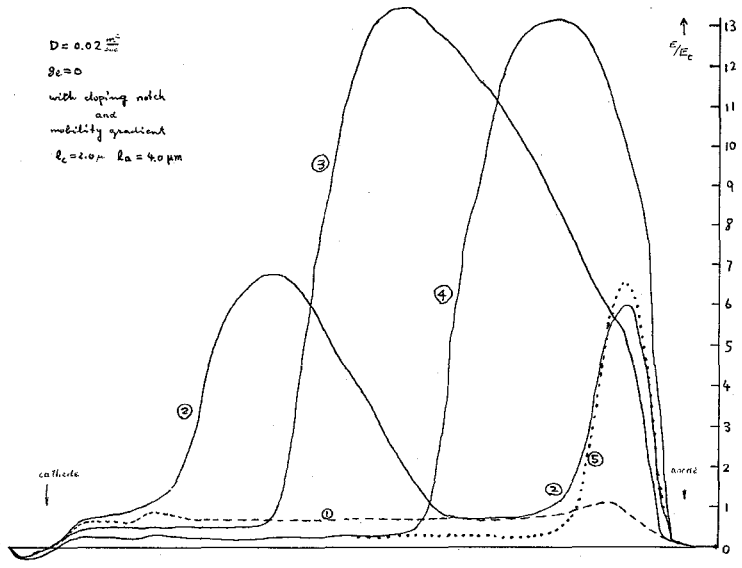

Fig. 14. Field profile for diode of Fig. 12 with mobility profile and doping notch (E—field, E_t—threshold field for the TE effect).

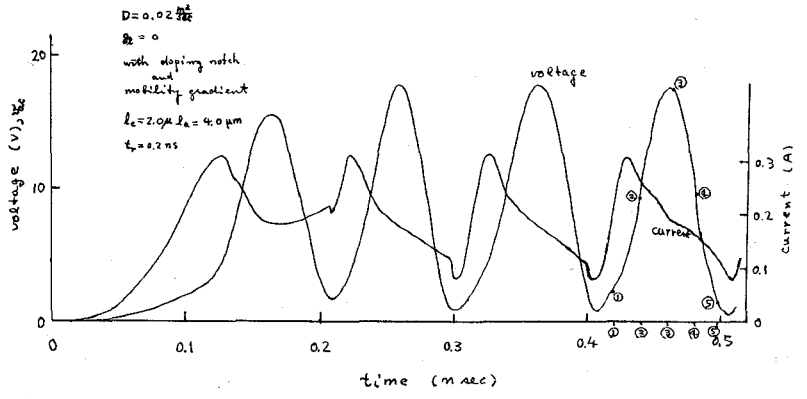

Fig. 15. Current–voltage transient of Fig. 14.

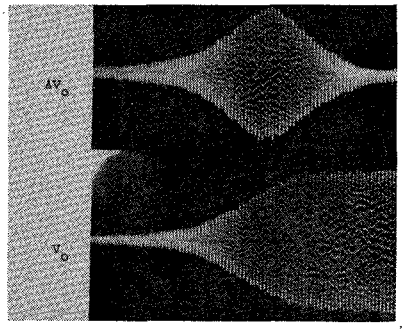

Fig. 16. Estimate of frequency change during transient by self-correlation technique. Top: sum Δv_o of incident and half-period delayed output signal during transient versus time. Bottom: output signal during transient versus time (vertical scales are arbitrary units). Time: 2 ns/div.

space-charge mode dependent, and thus also a function of the bias voltage. Any change in RF capacitance causes some operating frequency change. Fortunately, the equivalent inductance given by the shortened coaxial line also changes with frequency, and this can be made to counteract, to some extent, the frequency change due to the device reactance. To show this, the resulting frequency deviation for our experimental system is computed for a typical diode capacitance of 0.5 pF and for an increase in diode capacitance of 0.2 pF; a decrease in frequency of only 1.8 percent was found.

A direct measurement of the frequency shift during the buildup process has to be undertaken for each diode under investigation, and the following correlation technique has been used. As shown by Fig. 1, the output probe 1 is connected to a short coaxial line which is terminated by a short-circuit plunger. This plunger is adjusted so that the observed signal Δv_o at the entrance to the coaxial line at steady state is minimized. This means that the wave reflected by the short cancels the incoming wave because the return path delay is of half the period, or an odd multiple of this. Δv_o is then recorded for the transient by the sampling oscilloscope and the graph plotter. Fig. 16, top trace, is an example of the resulting wave function, which is caused by both the change in voltage amplitude and by any change in frequency.

A separate measurement (see Fig. 16, bottom trace) records the change in voltage amplitude directly, from which a function Δv_o is derived. Thus the derived Δv_o is compared with the measured Δv_o and any difference must be due to a change in frequency during transient. In our case, the measured value of Δv_o is always the same as the derived Δv_o,

within the experimental accuracy of our system. This means that the frequency change must be smaller than 25 MHz, so that it is justified to proceed with the constant-frequency assumption when using (1) for the determination of $g_d(v_{ac})$.

ACKNOWLEDGMENT

The authors wish to thank D. J. Colliver of the Royal Radar Establishment for his advice and help and for supplying the InP devices.

REFERENCES

[1] D. D. Khandelwal and W. R. Curtice, "A study of the single-frequency quenched-domain mode Gunn-effect oscillator," *IEEE Trans. Microwave Theory Tech.*, vol. MTT-18, pp. 178–187, Apr. 1970.
[2] M. Kawashima and H. Hartnagel, "New measurement method of Gunn-diode impedance," *Electron. Lett.*, vol. 8, p. 305, 1972.
[3] R. P. Owens and D. Cawsey, "Microwave equivalent-circuit parameters of Gunn-effect-device packages," *IEEE Trans. Microwave Theory Tech. (Special Issue on Microwave Circuit Aspects of Avalanche-Diode and Transferred Electron Devices)*, vol. MTT-18, pp. 790–798, Nov. 1970.
[4] J. C. Slater, *Microwave Electronics*. New York: Van Nostrand, 1950, p. 207.

An Experimental Study of Stabilized Transferred-Electron Amplifiers

ASHOK K. TALWAR AND WALTER R. CURTICE

***Abstract*—Experimental data are presented to describe various characteristics of stabilized transferred-electron amplifiers. The effect of bias voltage upon RF gain and linearity is shown. The conditions under which gain expansion is observed are described, and the importance of lattice temperature and RF signal strength in determining dc current is shown. All results are shown to be in good agreement with the large-signal theory for these amplifiers.**

INTRODUCTION

STABILIZED transferred-electron devices have been shown to be useful in obtaining broad bandwidth amplification at microwave frequencies [1], [2]. The devices and amplifiers are stable in the sense that RF oscillation does not occur when the input signal is removed. The observation of gain expansion [3] and unstable operation at certain values of bias voltage [1] have now been explained by a detailed large-signal analysis presented by Talwar [4] and Talwar and Curtice [5]. This paper summarizes the results of an experimental investigation of these effects and other experimental properties. It is shown that all properties are in agreement with the large-signal theory.

The method of theoretical analysis and some calculated characteristics of stabilized TE devices were presented by Talwar and Curtice [6] in 1971. It is assumed that the increased lattice temperature present in CW devices permits a stable electric field configuration to exist in the absence of external RF signals. Assuming specific external ac and dc current excitation, a set of one-dimensional large-signal differential equations is solved, progressing from the cathode contact. The effects of field-dependent diffusion are included as correction terms. Only dc and fundamental frequency RF electric fields are assumed to be important, whereas the effects of current harmonics are included. By integration of the electric field quantities over the total length of the device, the dc operating voltage and the RF impedance are obtained. The behavior of dc and RF impedance as functions of device parameters (including lattice temperature), operating bias, RF signal level, and RF signal frequency has been studied [4].

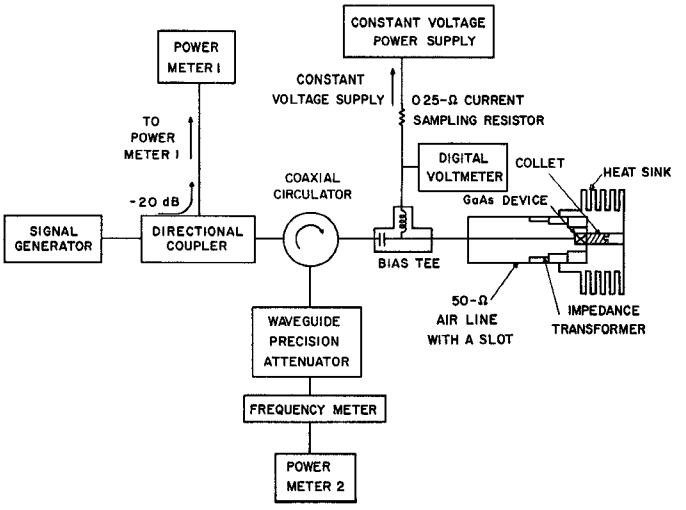

Fig. 1. Schematic diagram of the circuit used for the experimental study of stabilized TE amplifiers.

A. Description of the Circuit and the GaAs Diodes Used for the Experimental Study

A schematic diagram of the circuit used for most of the tests is shown in Fig. 1. The device is mounted in series with

Manuscript received November 6, 1972; revised February 26, 1973. This work was supported by the Air Force Systems Command, Rome Air Development Center, under Contract F30602-71-C-0099.

A. K. Talwar was with the Electron Physics Laboratory, Department of Electrical and Computer Engineering, University of Michigan, Ann Arbor, Mich. 48104. He is now with the Product Development Laboratories, Ford Motor Company, Dearborn, Mich. 48121.

W. R. Curtice was with the Electron Physics Laboratory, Department of Electrical and Computer Engineering, University of Michigan, Ann Arbor, Mich. 48104. He is now with the David Sarnoff Research Center, RCA Corporation, Princeton, N. J. 08540.